

12-2018

AUTOMATIC ERROR DETECTION AND CORRECTION IN LASER METAL WIRE DEPOSITION - AN ADDITIVE MANUFACTURING TECHNOLOGY

Adeola Idowu Adediran

University of Tennessee, adediran@vols.utk.edu

Recommended Citation

Adediran, Adeola Idowu, "AUTOMATIC ERROR DETECTION AND CORRECTION IN LASER METAL WIRE DEPOSITION - AN ADDITIVE MANUFACTURING TECHNOLOGY." Master's Thesis, University of Tennessee, 2018.
https://trace.tennessee.edu/utk_gradthes/5360

This Thesis is brought to you for free and open access by the Graduate School at Trace: Tennessee Research and Creative Exchange. It has been accepted for inclusion in Masters Theses by an authorized administrator of Trace: Tennessee Research and Creative Exchange. For more information, please contact trace@utk.edu.

To the Graduate Council:

I am submitting herewith a thesis written by Adeola Idowu Adediran entitled "AUTOMATIC ERROR DETECTION AND CORRECTION IN LASER METAL WIRE DEPOSITION - AN ADDITIVE MANUFACTURING TECHNOLOGY." I have examined the final electronic copy of this thesis for form and content and recommend that it be accepted in partial fulfillment of the requirements for the degree of Master of Science, with a major in Mechanical Engineering.

Lonnie J. Love, Major Professor

We have read this thesis and recommend its acceptance:

Sudarsanam Suresh Babu, Subhadeep Chakraborty, Chad Duty

Accepted for the Council:

Carolyn R. Hodges

Vice Provost and Dean of the Graduate School

(Original signatures are on file with official student records.)

**AUTOMATIC ERROR DETECTION AND CORRECTION IN LASER METAL WIRE
DEPOSITION – AN ADDITIVE MANUFACTURING TECHNOLOGY**

A Thesis Presented for the
Master of Science
Degree
The University of Tennessee, Knoxville

Adeola Idowu Adediran
December 2018

Copyright © 2018 by Adeola I. Adediran.

All rights reserved.

ACKNOWLEDGMENTS

The work described in this paper was jointly supported by the Manufacturing Systems Research group of the Manufacturing Demonstration Facility, Oak Ridge National Laboratory, GKN Aerospace, and the Bredesen Center for Interdisciplinary Research and Graduate Education, University of Tennessee.

ABSTRACT

Additive manufacturing (AM) technology involves building three-dimensional objects by adding material layer-upon-layer under computer control. Metal additive manufacturing offers new possibilities, not only in design, but also in the choice of materials. However, the additive process remains at a lower maturity level compared to the conventional subtractive processes such as milling, drilling and machining among others. Scientifically, there is a safety concern relating to the accuracy of the AM process, how printed products will perform over time and the consistency of their quality. Process accuracy and eventual part quality is compromised due to errors introduced by each of the building steps in the process.

Laser metal deposition with wire (LMD-w) is an additive manufacturing technology that involves feeding metal wire through a nozzle and melting the wire with a high-power laser. The technology is being largely researched for use in the aerospace industry to fabricate large aircraft components. With efficient process control, i.e. sensing, processing, and feedback correction of errors, the LMD-w technology has the potential to change the course of manufacturing. However, a prominent limitation in LMD-w is the difficulty in controlling the process.

This work proposes a method for detecting surface geometry errors in a deposited layer in the LMD-w process via laser height scanning and high-speed image processing. The controlled process is simplified into a linear system. The aim is to develop an effective sensing and correction module that automatically detects irregularities in each layer before proceeding to subsequent layers, which will reduce part porosity and improve inter-layer bond integrity.

TABLE OF CONTENTS

Chapter 1 INTRODUCTION.....	1
1.1 Causal factors to accuracy loss in metal additive manufacturing	4
Chapter 2 LITERATURE REVIEW.....	6
Chapter 3 MATERIALS AND METHODS.....	11
3.1 Research Question – High failure rates in additive manufacturing	11
3.2 Methodological Design	11
3.2.1 Error Definition.....	14
3.3 Modular sequence of automatic error detection and correction.....	15
3.3.1 Sensing Module	15
3.3.2 Processing Module.....	16
3.3.3 Correction Module.....	25
3.3.4 Controller design.....	31
Chapter 4 RESULTS AND DISCUSSION	36
4.1 Results	36
4.1.1 Results from open-loop bead width sensing.....	36
4.1.2 Results from closed-loop layer height sensing and correction	37
Chapter 5 CONCLUSIONS AND RECOMMENDATIONS.....	40
REFERENCES	42
VITA.....	46

LIST OF FIGURES

Figure 1-1 - A schematic diagram of the LMD-w process	2
Figure 3-1 - Width and height deviations	13
Figure 3-2 - Schematic representation of errors in bead width.....	14
Figure 3-3 - Schematic representation of errors in layer height	14
Figure 3-4 - Modular sequence of automatic error detection and correction	15
Figure 3-5 - Apparatus setup for melt pool imaging.....	17
Figure 3-6 - Apparatus setup for height measurement via optical profilometry.....	17
Figure 3-7 - Interactive ROI Extraction.....	20
Figure 3-8 - Schematic representation of the binarization process.....	20
Figure 3-9 - Image processing steps applied to a typical melt pool image.....	20
Figure 3-10 - Pre-deposition calibration	22
Figure 3-11 - Snapshot of the signal crossing detection program	23
Figure 3-12 - Layer height profiles from laser profilometer.....	23
Figure 3-13 - Filtered height scan with error regions highlighted	24
Figure 3-14 - Measurement data flow for automatic error detection and correction.....	25
Figure 3-15 - Simplified model of bead cross sections.....	26
Figure 3-16 - Illustration of a bead broken into 1-mm sections	29
Figure 3-17 - Pictorial representation of interactions between process variables	32
Figure 3-18 - LMD-w process Controller.....	33
Figure 3-19 - Expanded LMD-w process controller.....	35
Figure 4-1 - Bead width measurements	36
Figure 4-2 - Height scan obtained from laser scanner	38
Figure 4-3 - Error signal $e(t)$ representing height offsets	38
Figure 4-4 - Adjusted robot speed	39
Figure 4-5 - Combined height of the defective and corrected layer	39

CHAPTER 1

INTRODUCTION

Additive manufacturing is a technique for fabricating complex components layer by layer with great potential of decreased time and minimum materials waste compared with traditional subtractive manufacturing. The LMD-w technology in focus involves using a high-energy laser beam to melt metal wire into beads onto a substrate side by side and layer by layer. In the setup for this work, robotic controls are used to manipulate the laser beam-wire nozzle assembly and the melt pool along a 3D path. The melt pool then solidifies to form specific geometries as defined by the original CAD model. A schematic representation of the LMD-w process is shown in Figure 1-1.

The LMD-w process, which uses Ti-6Al-4V wire as the additive material, has gained attention in the aerospace industry due to its potential to significantly reduce stock material waste and save cost. In aircraft production, the use of laser metal deposition has two main benefits of cost and efficiency. Typically, large titanium forgings have significantly long lead times, and the machining process can be highly energy and material inefficient.

The average buy-to-fly ratio (BTF) in the fabrication of aircraft parts using traditional methods of subtractive manufacturing is 10:1. A BTF ratio of 10:1 means that about 10 pounds of stock material is required to make a 1-pound part, with 90 percent material discarded as scrap. BTF ratios even greater than 20:1 are a common occurrence^[1]. In contrast, additive manufacturing produces very little waste and reduces the cost of machining a block of material down to desired shape. LMD is cited as saving 90 percent of raw material at less than 10 percent of the cost of the same part produced through subtractive manufacturing. ^[2-4]

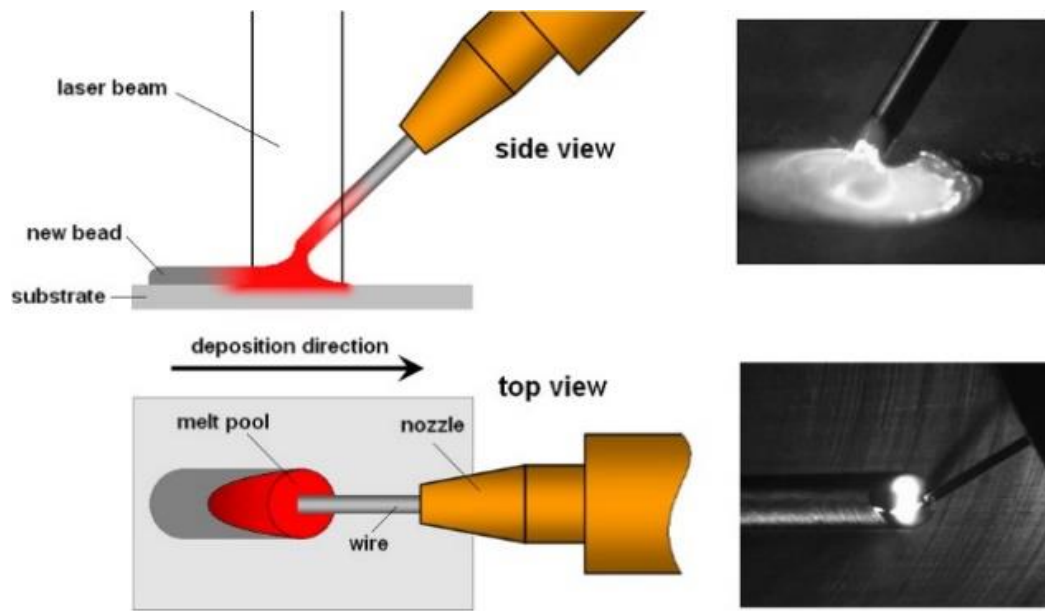


Figure 1-1 - A schematic diagram of the LMD-w process^[1]

Efficient control could help reduce lead time by as much as 80 percent, enable fabrication of parts having intricate shapes that maintain strength while significantly cutting the weight of the part by up to 40 percent.^[5]

Despite the potential benefits of this technology however, high component failure rates in additive manufacturing technology presents skepticism about the process due to the unpredictability of performance, which is vital for systems that are supposed to last decades and require components that need to have very low failure rates. The U.S. Air Force Research Laboratory (AFRL/ML) and the Metals Affordability Initiative (MAI) have identified that from a purely technical standpoint, an additive manufacturing technology cannot be considered for the manufacture of aircraft components unless the process is stable and controlled, and the resulting mechanical properties are well characterized and sufficiently invariable.^[6]

It is worthy of note that, in improving the accuracy of the additive manufacturing process and the quality of the printed part, reliable process control is first needed to ensure stable layer-to-layer deposition of material. Authors in Ref. ^[7] rightly argue that in order to achieve good process stability for multilayered deposition, continuous process monitoring and control of process parameters, such as the material feed rate, the heat input, and the travel speed is necessary. In Refs ^[8, 9] an empirical process model describing the relationship between the temperature and process parameters is designed to maintain a constant melt pool temperature. However, a drawback as stated in Ref.^[8] is that model parameters in metal additive manufacturing process change as the part is being built, making constant parameter models impractical.

1.1 Causal factors to accuracy loss in metal additive manufacturing

Identifying and quantifying system errors in metal AM systems is complicated not only because of the difficulty in separating machine characteristics from process characteristics, but also because the focus is on the machine itself. Different AM technologies often use dissimilar machine setups. ^[10] For example, processes that rely on laser beams often position the beam spot by deflecting the beam using two mirrors that may be independently rotated, while processes that rely on welding arc work by positioning an electrode within a short arc length, while preventing contact between the electrode and the workpiece. These systems differ widely from each other; however, some common concepts help to determine sources from which errors arise in the additive manufacturing process.

Firstly, additive manufacturing systems generally use X-Y-Z- coordinate axes in compliance with international standards ^[11, 12]. Secondly, the processes involve a feature being produced by positioning some machine component (an energy source, extrusion device etc.) relative to the position of the build platform. With these concepts in mind, flatness and straightness errors consisting of discontinuities in layers can arise from non-optimal settings on the system. Relatively small deviations from an optimal process setup, for example resulting from bad calibration, can lead to flaws of considerable magnitude, as underlined in the work presented in Ref. ^[13], and also as observed from the experiments in this study. Some of the characteristics of metal AM systems, as listed below, are critical for accurate part fabrication, and are consequently potential sources of errors.^[10]

- Errors in positioning of the laser beam (resulting from geometric errors of the two axes of rotation holding the laser beam positioning mirrors or form errors in the f - θ lens that focuses and shapes the laser beam spot)
- Geometric errors of the axis positioning the build platform
- Alignment errors between the axes
- Errors in the laser beam size and shape
- Variation in the beam power

Although outside the scope of this work, it is worth mentioning that powder-based systems also encounter faults from irregular powder size distribution, error in powder flatness, and transfer of porosity present in the metal powder to the bulk material of the finished part.

CHAPTER 2

LITERATURE REVIEW

Prior art in the field of automatic error detection and correction in metal additive manufacturing is studied in both sensing and feedback control aspects. On the part of sensing methodologies, systems employed are mostly ultrasonic, acoustic, optical and thermal. Some of the sensing techniques and technologies that have been explored in research and industry are discussed here.

Arc plasma visible emission has been explored in process inspection. In Ref. [14], an optical inspection system for monitoring the manual gas tungsten arc welding (GTAW) process is developed. The intensities of selected argon emission lines were measured, and the axial electron temperature of the plasma analyzed. A substantial variation of the temperature signal observed in the case of instabilities of the weld pool that cause weld defects was noted. A suitable algorithm, based on a statistical analysis of the signal, was subsequently developed to real time flag defective joints.

Digital cameras have also been useful in obtaining high resolution images which can be analyzed for useful information using image processing. Some studies have employed vision sensing using CCD cameras. In Ref. [15-17], a CCD camera placed coaxially to the laser beam follows and obtains images from the melt pool through a set of optics and mirrors. The images are used to analyze and compare cooling rates. In Ref. [18], a passive vision sensor system consisting of a CCD camera, a narrow-band and neural filter, and placed opposite the welding nozzle, is designed to observe the nozzle-to-top-surface-distance (NTSD) directly.

Weld-pool depth analysis has also been carried out in Ref. [19]. In the study, an integrated welding/sensing system is proposed to provide a method to conduct precision gas tungsten arc

welding with weld pool surface feedback. A novel non-transferred plasma charge sensor is proposed to measure the depth of the weld pool surface. A flat surface is periodically established to provide a real-time reference. The main-arc-on period is selected as the system's input. Because of possible large variations/ranges in manufacturing conditions, an interval model control algorithm with updated intervals is adopted.

A 3D laser scanner is utilized in Ref. [20] to obtain a 3D height profile of the manufactured part after each deposited layer. The work utilizes the principle of optical triangulation, i.e. a laser line is projected on to the target surface and the reflected light is captured by a two-dimensional sensor from which a single-line height profile is calculated. An iterative learning controller adjusts the wire feed rate based on the 3D scanned data of the printed part. A circular laser three-dimensional (3D) scanner is also developed in [21] instead of a one-dimensional laser spot scanner (1D) and two-dimensional (2D) striped laser light. The vision sensor consists of a charge-coupled device (CCD) image sensor and light scanning system based on a rotating lens that generates a circular laser beam. Using the proposed circular laser scanner, a seam tracking system is constructed, and architecture based on the Visual C++ and RAPID languages which determines the cooperation among image processing modules is carried out.

Temperature monitoring and regulation has also been investigated. Heat input regulation is crucial for deposition quality in laser metal deposition (LMD) processes. To control the heat input, melt pool temperature is regulated using temperature controllers. [9] A closed-loop controller is employed using feedback from the monitored temperature of the part being printed. Deviations between the set and measured temperatures are used to adjust the energy source power and achieve a homogeneous temperature distribution and better dimensional accuracy. In

[22, 23] a photodiode is integrated with the processing head of the machine and its signal used as input to the controller.

Displacement sensors have been employed in detecting surface irregularities by measuring the displacement of points on a layer profile against a set reference. The use of displacement sensors is presented in Ref. [8, 9], where the melt pool temperature is controlled using a setup consisting of a pyrometer as temperature sensor and a laser displacement sensor (OMRON model Z4M-W100) to measure track height profile. Both temperature and height profile of each layer were analyzed and controlled. Boddu et al. [24] uses a setup comprising a pyrometer, a displacement sensor, and a coaxial CCD. Information from this setup was used to control the process and improve surface finish, cold spots, and porosity.

Thermal imaging has also been investigated and is being widely employed for its promising results. A study conducted in Ref. [25] reveals that the vast majority of research on process monitoring and control in metal-based AM focuses on temperature monitoring in powder bed fusion and direct energy deposition processes. This is because temperature has a direct impact on the mechanical properties of the part being printed, and thus stands as a valuable representation of the eventual part quality. Authors in Ref. [13] demonstrate a good correspondence between the flaws visible in images recorded of a Selective Electron Beam Melting (SEBM) build using an IR camera and the flaws recorded by traditional metallographic sectioning of the samples after the process was finished. This was based on the principle that every area of (strikingly different) heat radiation corresponds to a flaw, most likely due to the convex shape of the formed pores which locally changes the emissivity of the surface.

The work presented in Ref.^[26] also employs thermal imaging technique to observe the temperature distribution of a complete layer and consequently study the process errors originating from insufficient heat dissipation as well as the limits for detecting pores and other irregularities. The total melt pool area as well as the length-to-width ratio is identified to be the relevant detection variable when analyzing process errors. In-Process monitoring is also done in related processes like Selective Laser Sintering (SLS) of plastics or Electron beam melting (EBM) of metals. Arcam, a company which sells EBM manufacturing systems, develops a camera-based surveillance tool. The system will feature a custom image evaluation software and an IR camera that is integrated into the building chamber. However, a downside reported in Ref. ^[13] in using an IR camera is that the resolution of the camera sets certain limits to the interpretation of the images.

Hu et al. ^[27, 28] also capture images from the melt pool with a thermal imaging system using an IR high speed camera positioned coaxially with the laser beam. Information from the analysis of the captured images is then fed to a controller and used to adjust the laser power to ensure uniform temperature distribution.

Experimental efforts have also been made towards automated error compensation through feedback action on certain process-specific error signals. In Ref. ^[29] a camera-based monitoring system is developed for closed loop control of straight-bead deposition and in Ref. ^[30] a temperature monitoring system is investigated for a laser metal-wire deposition process. Xiong et al ^[18] also describes using a passive vision sensor system to monitor the nozzle-to-top-surface distance (NTSD) and an adaptive controller to keep the NTSD constant in a gas metal arc welding (GMAW) process. Deviations in the NTSD were compensated by the movement of the working flat and the adjustment of the deposition rate on next deposition layer. The controlled

process was simplified into a linear system, and an adaptive control system was designed to keep the NTSD constant. Similarly, in Ref. [20], a 3D scanning system is developed and integrated with the robot control system for automatic in-process control of the deposition. An iterative learning controller was designed in a laser metal-wire deposition process to control layer height with deviations in the layer height compensated by controlling the wire feed rate on next deposition layer, based on the 3D scanned data. Ref. [13] further suggests re-melting of compromised area, as well as additional material deposition + re-melting.

The area of interest for this work is in metal wire feed processes, and besides the above-mentioned references however, not much investigation has been carried out yet on the side of metal wire-feed systems in the literature. By contrast, powder-based systems have been researched extensively and several publications have resulted from these works. For example, monitoring and process control using cameras [27, 31, 32], closed-loop height control using photodiodes [22, 33-35], powder flow control based on motion system speed profile [36], temperature measurements using pyrometers [37-39]. However, these results cannot be simply transferred to wire-based deposition systems since the two processes are dissimilar in many ways.[20] LMD-w has the advantages of higher deposition rates, wider availability of wire products, and cheaper feedstock over powder counterparts[40]. Thus, it is worthwhile to investigate process control for laser metal wire processes in depth.

CHAPTER 3

MATERIALS AND METHODS

3.1 Research Question – High failure rates in additive manufacturing

This research stems from the safety concern relating to the accuracy of the additive manufacturing process and the consistency of the quality of printed parts. Process accuracy and eventual part quality is compromised due to errors introduced by each of the building steps in the process. One approach to managing the risk of part failure in additively manufactured parts from the industry end is optimization of the manufacturing process, specifically increasing accuracy by eliminating some of the errors that arise in the printed part. Accuracy in additive manufacturing is generally evaluated by dimensional errors, form errors and surface roughness of manufactured parts. Form errors are further classified into cylindricity errors, staircase errors and flatness/straightness errors. The focus of this work will be on flatness and straightness errors. The flatness error of a nominal flat feature is defined by ASME as the minimum tolerance zone between two offset planes which completely enclose the points sampled from the manufactured feature. Attention is directed specifically at surface roughness and discontinuities in the layered build. The aim is to incorporate in-process detection and correction of discontinuities, thus enabling capability to detect gaps and holes in each layer before proceeding to subsequent layers.

3.2 Methodological Design

In the LMD-w process, key process variables have been identified as useful pointers for the resultant bead geometry i.e. bead width and height. These variables include: i) Laser power ii)

Wire speed iii) Robot travel speed iv) Nozzle-to-top-surface distance iv) Wire offset from melt pool

Experimental work on the deposition of Ti-6Al-4V using the LMD-w process at the Oak Ridge National Laboratory's Manufacturing Demonstration Facility has shown that the width of a bead has a direct relationship with the laser power. Thus, higher powers typically result in wider, flatter beads, while lower powers yield narrower, taller beads. Similarly, the height of a bead is a function of the material deposition rate; i.e. how much metal wire is fed into the melt pool per unit time, or per unit distance. This in turn is directly proportional to the wire feed rate at constant robot speed, or inversely proportional to the robot travel speed at constant wire feed rate.

In studies of wire-fed systems, the geometry of each bead has been shown to provide predictive information about the properties and quality of the final manufactured part. ^[25] These properties include density, dimensional accuracy, surface finish, and mechanical properties. The interrelationship thus suggests that these properties can be steered toward the desired results through accurate monitoring and control of the constituent bead geometries, using the above key process variables as feedback control signals during the build process. Essentially, the ideal outcome is a perfectly straight bead profile, i.e. that each bead has straight-line edges and maintains a set horizontal width (x-axis) and vertical height (z-axis) at a constant value throughout the y-axis travel of the manipulator while executing a layer. Deviations from the target bead width and height are then flagged for determining the necessary corrective actions to restore the geometries to desired values (Figure 3-1).

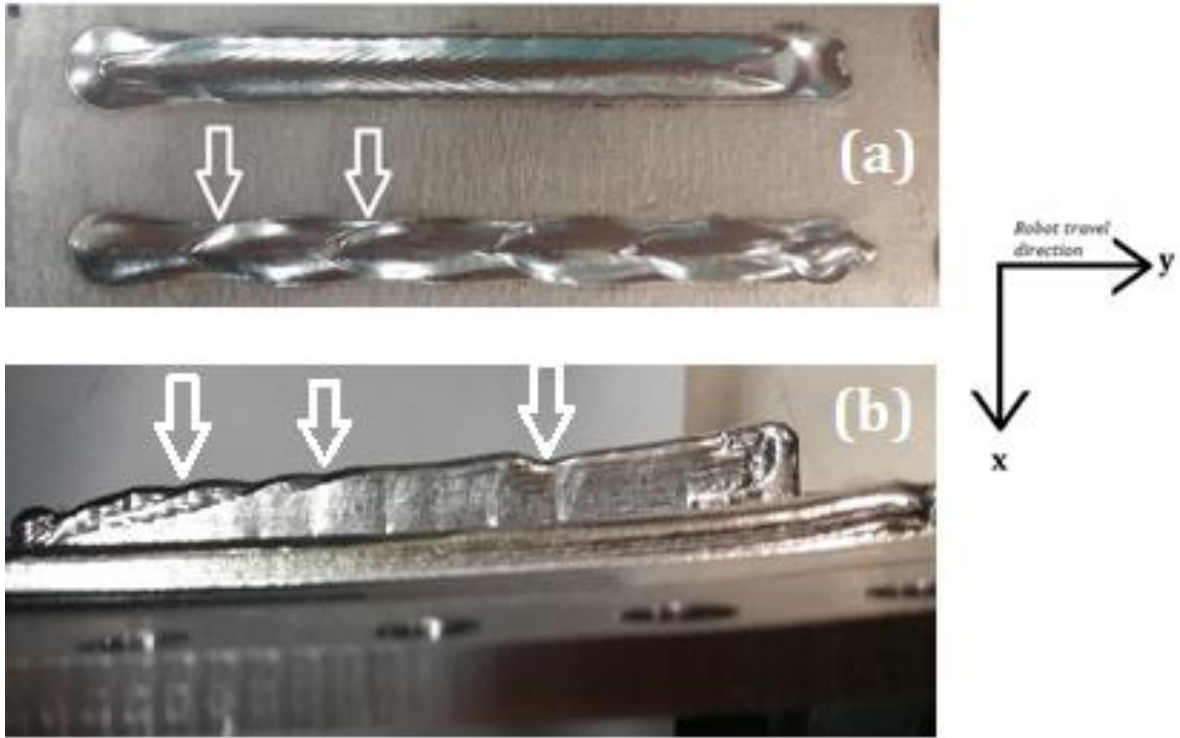


Figure 3-1 - Width and height deviations

- a. Discontinuities in the x-y plane
- b. Discontinuities in the y-z plane

3.2.1 Error Definition

An “error”, as used in this writing, is a distance deviation from a reference point. In the context of width measurements, an error refers to a positive or negative difference between the measured width of a bead on any layer n and a reference width value set to be equal or relative to the ideal width of that layer. A positive error, or a ‘neck’, refers to an indentation in the profile, while a negative error, or a ‘bulge’, refers to an outward protrusion in the profile, as shown in Figure 3-2. Similarly, in the context of height measurements, an error refers to a positive or negative difference between the measured height of a layer n and a reference height value set to be equal or relative to the ideal height of that layer. A positive error, or a ‘dip’, refers to a downward depression in the profile, while a negative error, or a ‘bump’, refers to an outward protrusion in the profile, as shown in Figure 3-3.

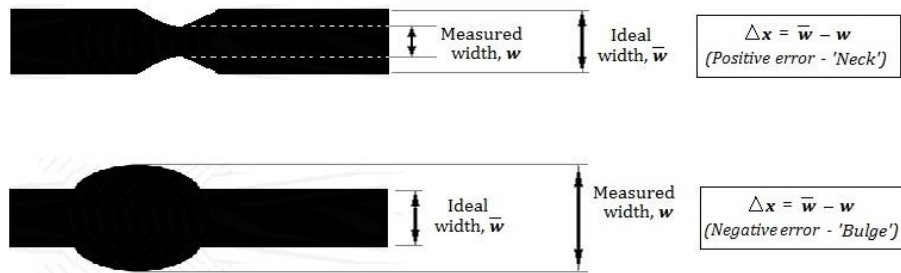


Figure 3-2 - Schematic representation of errors in bead width

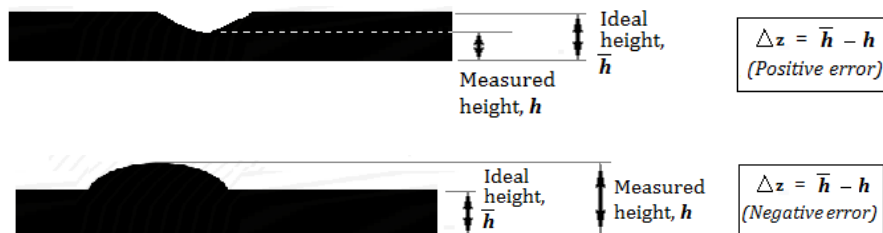


Figure 3-3 - Schematic representation of errors in layer height

3.3 Modular sequence of automatic error detection and correction

The error detection and correction process is implemented in three modules (Figure 3-4):

- A. Sensing
- B. Processing
- C. Correction

3.3.1 Sensing Module

The sensing module deals with the initial detection of layer width and height errors. There are various possible means by which errors can be detected, including ultrasonic, acoustic, optical and thermal sensors. However, in this work, high resolution optical imaging is used for open-loop bead width monitoring, while laser scanning is used to monitor layer height. In the sensing module, bead width and height data are collected by the system. Location data is also collected to specify points on the build where the errors occur.

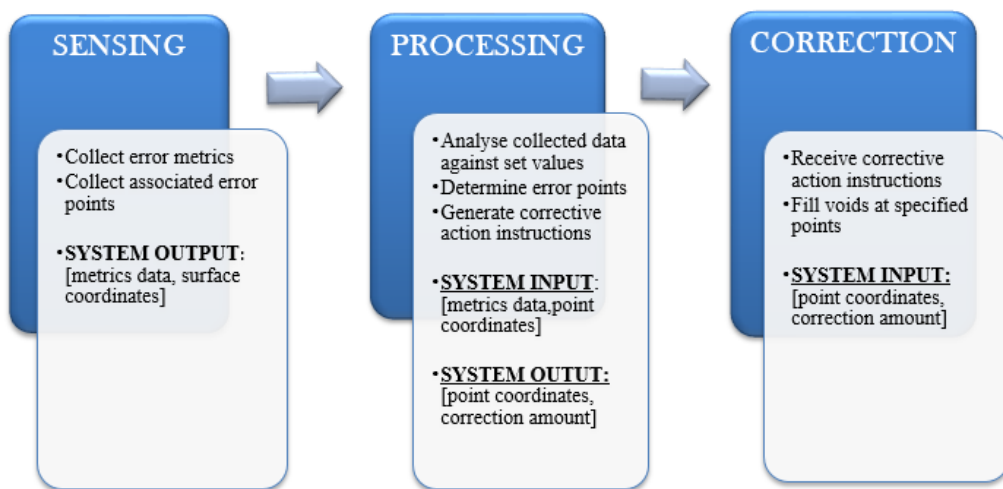


Figure 3-4 - Modular sequence of automatic error detection and correction

3.3.1.1 Bead Width Monitoring Via Image Processing

The goal of the sensing approach described in this section is to be able to view the melt pool in-process and to accurately detect deviations in the width of the pool along the bead. Due to the extreme brightness of the melt zone in the LMD process, visualizing the melt pool is done via a high-definition CMOS-based camera equipped with cascaded neutral density filters to significantly attenuate the intensity of the melt pool. The camera was mounted coaxially with the laser optics in a setup as shown in Figure 3-5.

3.3.1.2 Layer Height Monitoring Via Optical profilometry

In the height sensing approach described in this section, a laser profilometer is employed to take surface profiles of deposited beads from which height offsets from target height are recorded. The setup is shown in Figure 3-6.

3.3.2 Processing Module

The processing module is the interface between the sensing system and the correction system. This stands as the center of data analysis and involves programmatic computation on the data collected in the sensing module. In this phase, variables are defined and the term “error” quantified, to enable the system to identify a discontinuity, the occurrence point, and the degree (depth/width) of the discontinuity. The processing module then passes corrective instructions to the repair system, based on the analysis performed.

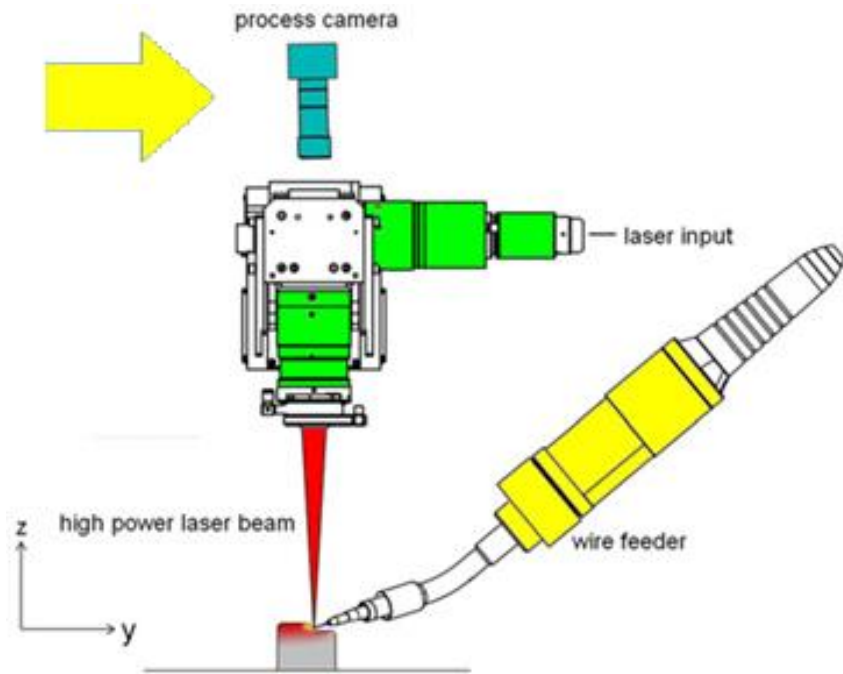


Figure 3-5 - Apparatus setup for melt pool imaging

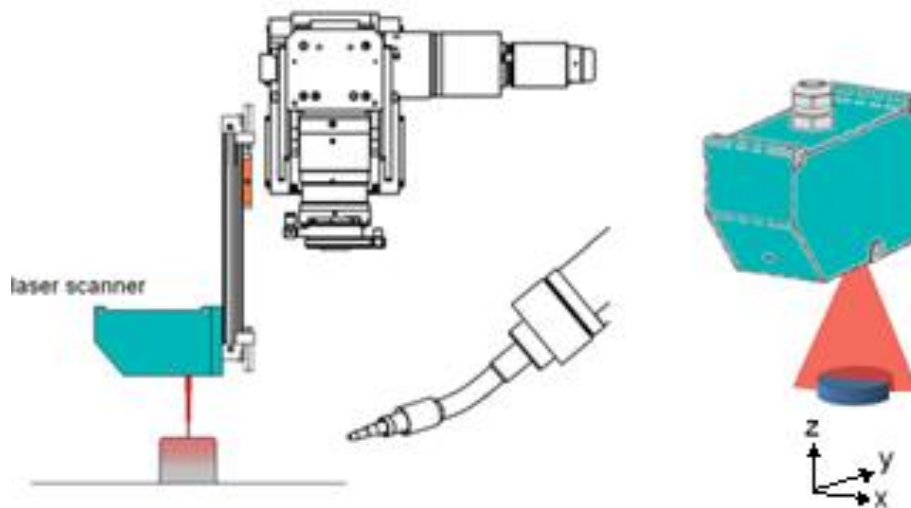


Figure 3-6 - Apparatus setup for height measurement via optical profilometry

Output data from this system includes the following:

- Location data (specifying points at which to implement correction)
- Quantified correction degree (such as amount of additional or deducted material to be deposited at each point of occurrence)
- Sequence in which to carry out the correction.

The processing system is designed in the form of a computer serving as the center of the control system to implement functions including control of the movement of the deposition assembly (wire extruder and laser bead) using a data acquisition card, optical image display and processing, on/off control and intensity adjustment of the laser beam, speed adjustment of the wire feed, and a human–machine interface to provide the user with necessary information.

For this system, multiple programming software were employed. National Instruments Data Acquisition system (NI DAQmx) was used to acquire measurement data from the laser height scanner. MATLAB image processing toolbox was used to extract characteristic image information from the weld pool monitoring camera. The feedback control which adjusts input variables using height deviations from the nominal value was modeled and simulated both in MATLAB and LabVIEW environments. The user interface which enables the user to command and receive state feedback from the system was designed using NI LabVIEW Graphical Programming.

3.3.2.1 Processing of Bead Width Measurements

Optical images were extracted from recorded videos of each bead in the form of image frames. An image processing algorithm was developed using MATLAB software to process the extracted frames and identify the bead geometry in the following five steps: i) Region of Interest

Extraction, ii) Binarization, iii) Noise extraction, iv) Geometry measurement, and v) Data Conversion & Logging

- i. Region of Interest (ROI) Extraction – a portion of the entire frame is defined, on which filtering and further processing will be done (Fig. 3-7). This is necessary to isolate the melt pool region as it contains the useful visual information, while the rest of the frame is redundant. This saves computing power and processing time.
- ii. Binarization – A typical frame obtained from the ROI extraction is essentially an RGB (Red-Green-Blue) image or true color image. An RGB frame is stored as an m-by-n-by-3 data array of pixel defining red, green, and blue color components for each individual pixel. The true color image is converted to a grayscale image in which the value of each pixel carries only intensity information. The grayscale image contains varying shades of gray from 0 to 255, with black being the weakest intensity (0) and white being the strongest (255). These pixel intensity values are compared against a defined threshold that sets pixels within its range to 1 and all others to 0. Figure 3-8 shows a sample binarization with a threshold value of 100. The resulting image is an array of 0s and 1s, where a 0 is a black pixel and a 1 is a white pixel. With this process, the boundary of the melt pool region is extracted.
- iii. Noise extraction – Occasional unwanted noise in acquired images is a common occurrence in the LMD process and needs to be filtered out to prevent false interpretation of image data by the algorithm. Noise is identified in the binary image as small clusters of white pixels or ‘1’ values in the array that are significantly smaller in area in comparison to with the actual melt pool, as depicted in the bottom-right image of Figure 3.9. The filtration is done by setting all such clusters to ‘0’, essentially turning them to black.



Figure 3-7 - Interactive ROI Extraction

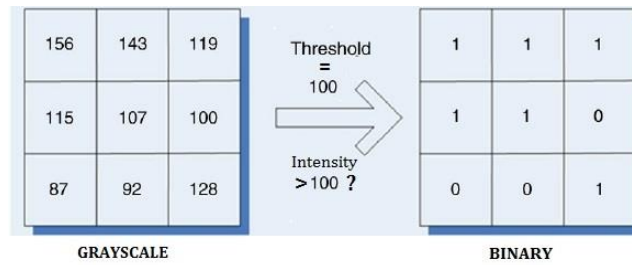


Figure 3-8 - Schematic representation of the binarization process

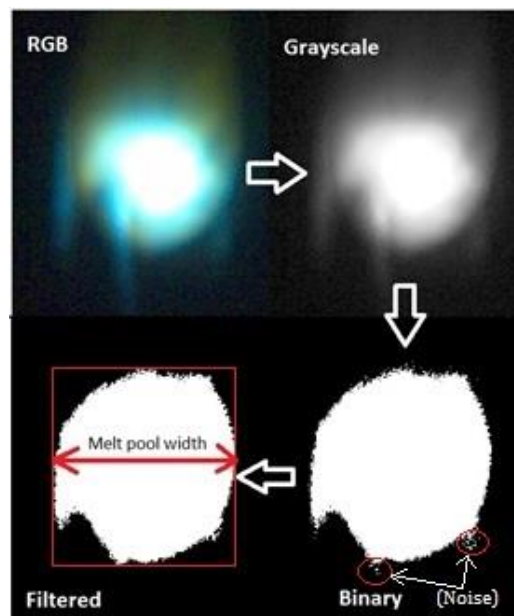


Figure 3-9 - Image processing steps applied to a typical melt pool image

- iv. Geometry measurement – In this process, the needed measurements of bead width are extracted, i.e. the horizontal distance between the edges of the melt pool. The width of the bead is measured as the width of the smallest rectangle binding the image of the melt pool as shown in Figure 3-9.

- v. Data Conversion & Logging – Raw geometry measurement data is initially presented in pixel units. The conversion to distance units is done at this stage. The converted values are then compared with the target value of the melt pool width from which error (‘neck’ and ‘bulge’) points are logged.

3.3.2.2 User-Interactive Thresholding

When monitoring the melt pool in the LMD process, determining the exact bounding region of the melt pool is sometimes a challenge because each build job mostly features different parameters and process disturbances. Even under identical process conditions, changes in camera settings, such as focus and filtering, could occur. These factors may make the melt pool appear different from build to build. The user-interactive thresholding concept is introduced to allow pre-build calibration to teach the monitoring system to correctly identify the melt pool prior to the start of the actual build process. To implement this, a test bead is run, and the calibration is done via visual judgement of the operator, i.e. the threshold, as discussed in the binarization stage above, is set by interactively tuning intensity parameters and visually observing the response until a satisfactory match between visually observed and computer-detected melt pool region is achieved. It should be noted that for best results, a suitable camera capable of providing

clearly discernable images of the melt pool is necessary. Several studies have already been conducted on visualization of melt pools in laser deposition and welding processes. [\[41-46\]](#)

Figure 3-10 shows images in the pre-build calibration. In (a), the threshold is set too low resulting in a detected ‘pool’ far out from the actual melt pool. In (b), the threshold is set too high and does not capture the entire melt pool. Figure 3-10(c) shows a satisfactory setting.

3.3.2.3 Processing Layer Height Measurements

A Keyence laser height scanner was used to acquire layer height measurements. Figure 3-11a shows a typical output scan in which the nominal height value is set to 1mm. To eliminate signal noise and also prevent excessive correction frequency, a second order Butterworth lowpass filter was applied to smoothen the signal, resulting in Figure 3-11b.

In the corrective approach designed in this work, height offsets were extracted, and the filtered signal programmatically split into regions of distinct ‘voids’ and ‘bumps’ (Figure 3-11). Regions are detected when the signal crosses the nominal value (red line in Figure 3-12a – b), resulting in the shaded regions of Figure 3-13. The heights in each segment are fed to the controller as an error signal which is used to adjust the input for the subsequent layer.

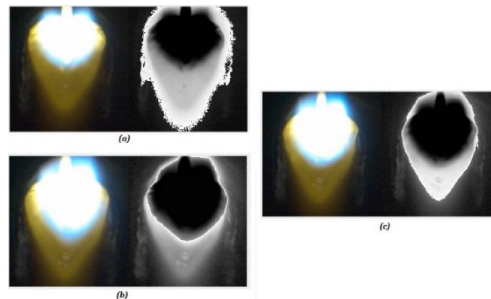


Figure 3-10 - Pre-deposition calibration

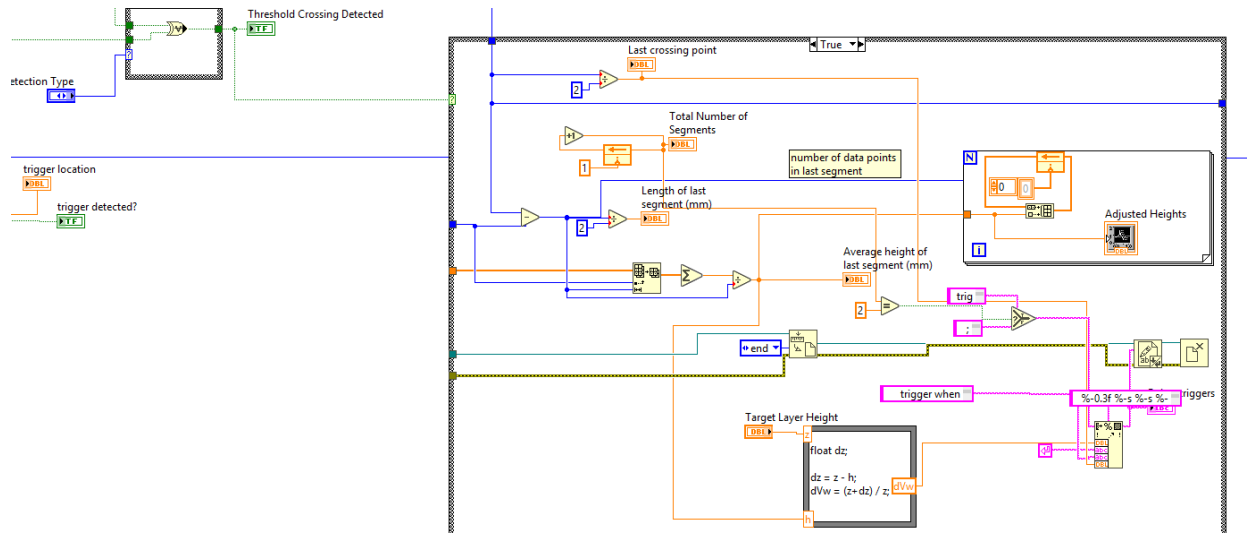
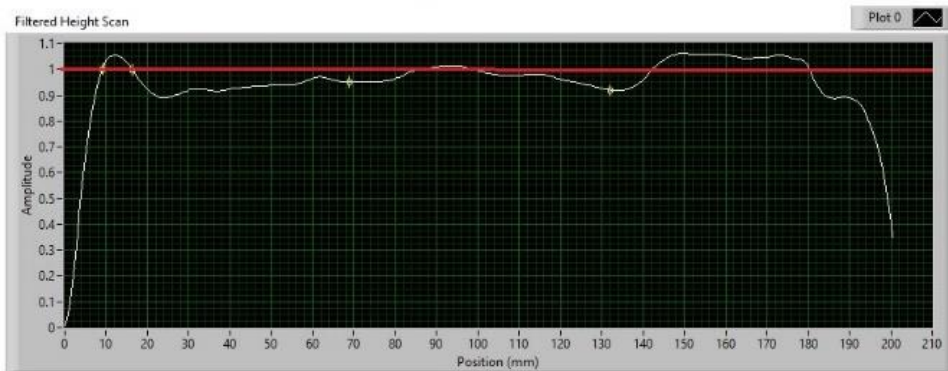


Figure 3-11 - Snapshot of the signal crossing detection program



(a)



(b)

Figure 3-12 - Layer height profiles from laser profilometer

- a) Raw height scan
- b) Filtered height scan

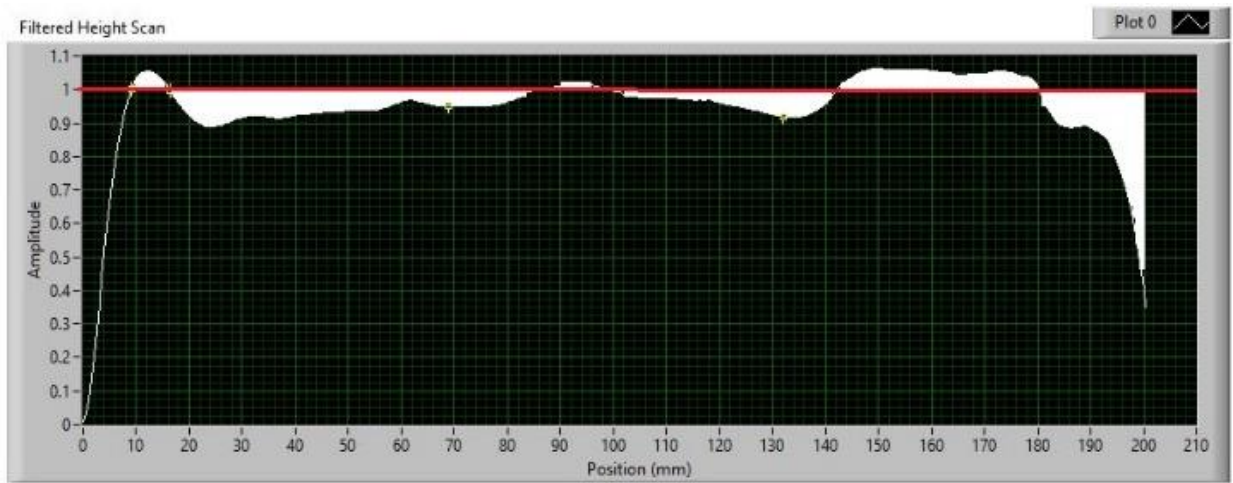


Figure 3-13 - Filtered height scan with error regions highlighted

3.3.3 Correction Module

Having acquired measurement data in terms of bead width and layer height from the sensing module, height offsets were extracted and fed into the control module. The flow of data is shown in Figure 3-14.

In the correction module, a model for the correction of the height deviations was derived. A proportional controller was designed to identify and regulate the process parameters to compensate for these deviations. The control system was designed to correct current layer errors during the deposition of the next layer, and follows the form;

$$u_{n+1} = u_n + K * e_n$$

Where u_n is the input to the system during the n th repetition (or layer), e_n is the tracking error during the n th repetition and K is a design parameter representing operations on e_n

Error correction in form of adding (or deducting) filler material at regions where discontinuities occur was explored, with the amount of filler material required at each point having been determined by the processing module.

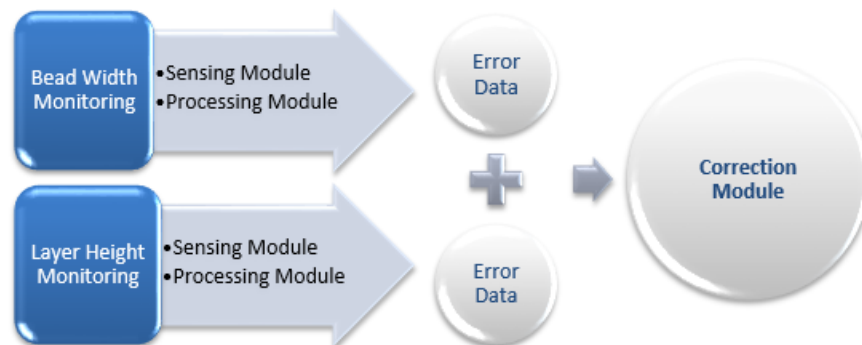


Figure 3-14 - Measurement data flow for automatic error detection and correction

3.3.3.1 Mathematical Calculations

Notations

d	-	Wire diameter
A_w	-	Wire cross-sectional area
A_b	-	Bead cross-sectional area
v_w	-	Time-varying wire feed speed ('t' notation suppressed for simplicity)
v_w'	-	Nominal wire feed speed
v_r	-	Time-varying robot travel speed ('t' notation suppressed for simplicity)
v_r'	-	Nominal robot speed
P_l	-	Laser power
x	-	Bead width
y	-	Robot traverse distance
z	-	Target height of current layer

For simplicity of initial calculations, a rectangular bead cross-sectional shape is first assumed, as shown in Figure 3-15.

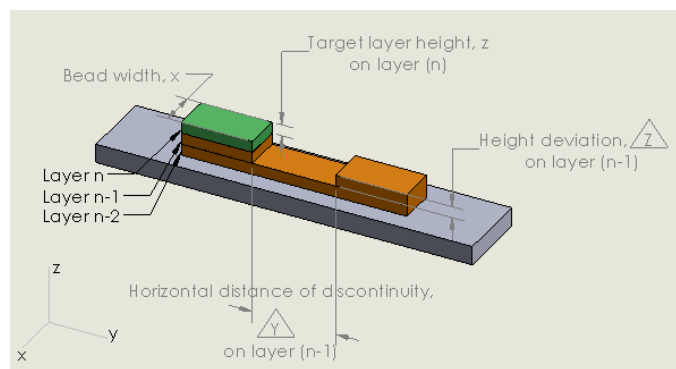


Figure 3-15 - Simplified model of bead cross sections

Three layers are depicted in the figure above, each with a target height z . Layer (**n-2**) is assumed to be without defect while layer (**n-1**) contains a void of depth Δz over a horizontal distance Δy . The goal is to fill in this void while depositing layer **n**. To derive the amount of material needed for correction, and ultimately the adjusted travel speed, it is necessary to first derive the material deposition rate with respect to the wire feed speed and robot travel speed.

3.3.3.2 Derivation of material deposition rate and bead cross-sectional area

The cross-sectional area of a deposited bead, A_b , is a function of material deposition rate. The volumetric flow rate, F , i.e. the volume of molten metal deposited per second, is calculated as:

wire cross-sectional area \times wire feed speed

$$\therefore F = A_w \cdot v_w \text{ (in cubic millimeters per second)} \quad (3-1)$$

Therefore, at set robot speed v_r' , the deposition rate σ' per unit distance of horizontal travel is:

$$\text{Deposition rate (volume of material per mm)} = \frac{A_w \cdot v_w'}{v_r'} \quad (3-2)$$

3.3.3.3 Derivation of robot speed and wire speed correction

To compensate for previous layer (**n-1**) void on current layer (**n**), the ideal volume of the current layer and volume of the void are considered. In figure 3-13, let ideal volume = $(x \times \Delta y \times z)$, and void volume = $(x \times \Delta y \times \Delta z)$, then

$$\text{void volume} = \left(x \times \Delta y \times z \times \frac{\Delta z}{z} \right) = \frac{\Delta z}{z} \times \text{ideal volume}$$

$$\therefore \text{Volume to deposit on current layer (over } \Delta y) = \text{void volume} + \text{ideal volume}$$

$$= \left(\frac{\Delta z}{z} + 1\right) \times \text{ideal volume}$$

$$V = \left(\frac{\Delta z}{z} + 1\right) \times (\text{bead cross-sectional area} \times \text{linear travel distance})$$

$$V = \left(\frac{\Delta z}{z} + 1\right) \times A_b \times \Delta y$$

Time to deposit volume V is $\frac{V}{F}$

$$= \left[\frac{\left(\frac{\Delta z}{z} + 1\right) \times A_b \times \Delta y}{(A_w \times v_w')} \right] \text{secs}$$

Therefore, to fill the void volume, the new deposition rate (volume per distance) over void distance Δy needs to be $\frac{\text{volume to fill}}{\text{distance to fill}} = \frac{V}{\Delta y} = \left(\frac{\Delta z}{z} + 1\right) \times A_b$.

$$\sigma(t) = A_b \cdot \left(\frac{\Delta z}{z} + 1\right) \quad (3-3)$$

Recall from equation (3-2) that the steady state deposition rate σ' per unit distance of horizontal travel is $\frac{A_w \cdot v_w'}{v_r'}$. This means that the volume of material in each 1-mm section, $(A_b \times 1) = \frac{A_w \cdot v_w'}{v_r'}$, as illustrated in Figure 3-16.

If uniform cross-sectional area is assumed across the entire bead length, then the cross-sectional area of the bead can be taken as equal to the volume of material per unit distance, thus:

$$A_b = \sigma' = A_w \times \left(\frac{v_w'}{v_r'}\right) \quad (3-4)$$

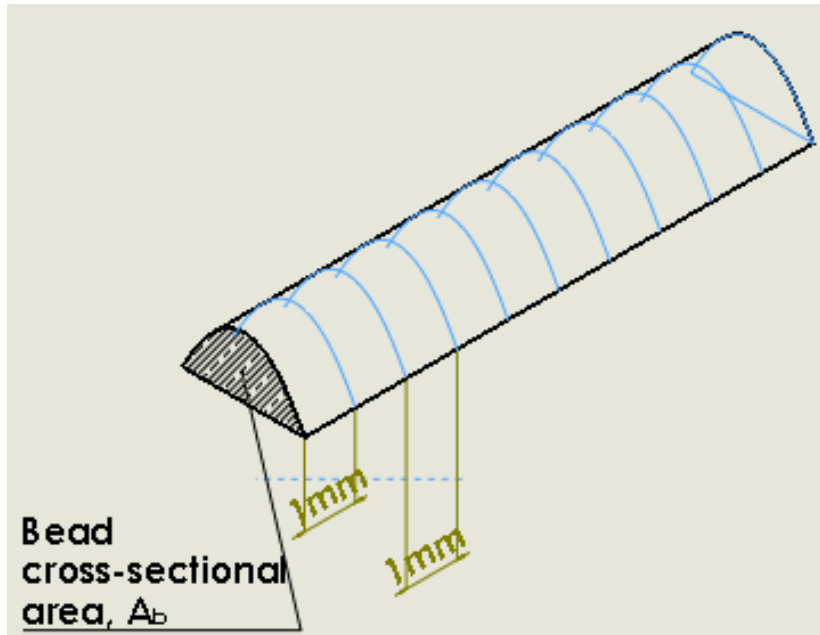


Figure 3-16 - Illustration of a bead broken into 1-mm sections

Substituting equation (3-4) into equation (3-3), we have

$$\sigma(t) = \sigma' \cdot \left(\frac{\Delta z}{z} + 1 \right)$$

$$\left(A_w \times \frac{v_w}{v_r} \right) = \left(A_w \times \frac{v_w'}{v_r'} \right) \cdot \left(\frac{\Delta z}{z} + 1 \right)$$

$$\boxed{\frac{v_w}{v_r} = \left(\frac{v_w'}{v_r'} \right) \cdot \left(\frac{\Delta z}{z} + 1 \right)} \quad (3-5)$$

Equation (3-5) is the wire speed/travel speed ratio that needs to be maintained to implement height corrections while depositing a subsequent layer.

It should be noted that v_w , v_r and Δz are time-varying signals where the '(t)' notation has been suppressed for simplicity. Thus, $\Delta z(t)$ is the error signal obtained by subtracting the laser height scan signal h of the previous layer from the constant nominal height, z .

$$\Delta z(t) = z - h$$

From equation (3-5), we can choose to vary both variables while keeping the ratio as defined or keep one variable constant at the nominal value and vary the other. Thus, at constant wire feed speed $v_w = v_w'$, the adjusted robot speed v_r is

$$v_r = \frac{1}{\left(\frac{\Delta z}{z} + 1 \right)} v_r'$$

$$v_r = \frac{1}{\left(\frac{\Delta z}{z} + 1 \right)} v_r'$$

$$v_r = \left(\frac{z}{z + \Delta z} \right) v_r' \quad (3-6)$$

Similarly, at constant robot travel speed $v_r = v_r'$, the adjusted wire speed v_w is

$$v_w = v_w' \cdot \left(\frac{\Delta z}{z} + 1 \right) \quad (3-7)$$

3.3.4 Controller design

As derived in Equations (3-6) and (3-7), height control in the LMD-w plant can be implemented by adjusting the wire feed speed and/or robot travel velocity. In this work, the robot travel speed is chosen as the control variable. Figure 3-17 shows the interaction between the LMD-w key process variables.

It has been found over a series of experiments that once a set of optimal wire feed parameters (position of wire tip relative to the laser beam spot and wire vertical offset from the nozzle) have been established for steady state deposition, it is best to keep these variables unchanged, as even very slight variations in these values along a bead and between layers have been observed to cause very undesirable results of droplet formation or wire being welded onto substrate.

Furthermore, in terms of hardware capability, the wire feeder is prone to several process deviations that can upset the accuracy of response to wire feed manipulation commands. The wire feeder is digitally controlled, and features roller drives which give room for slippage.

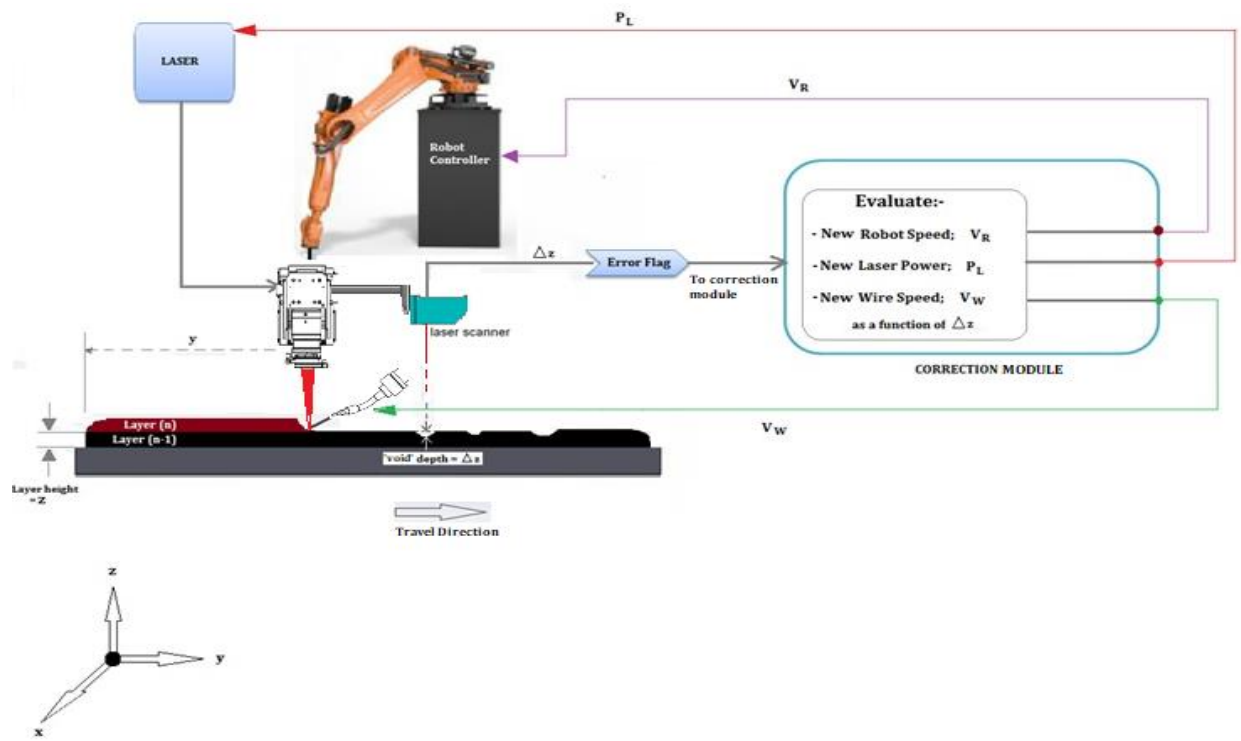


Figure 3-17 - Pictorial representation of interactions between process variables

Deformation of wire can also occur as a result of pressure forces. Therefore, further manipulation of wire feed during the build process is likely to lead to an accumulation of faults from multiple sources.

For the problem at hand, minimal process disruption is desired. Thus, the robot speed is chosen as the more suitable control variable. The 6-DOF KUKA CR-90 robot in this setup belongs to a class of robots with the highest accuracies in the market, with a repeatability of +/- 0.05mm.

3.3.4.1 Linearized LMD-w Plant, $h = f(v_r)$

In this section, we derive a function to describe the LMD-w plant, i.e. $h = f(v_r)$, in the feedback loop shown in Figure 3-18, where h is the corrected output height $z + \Delta z$.

Equation (3-6) gives the relationship between the input robot speed v_r , where v_r' is the nominal robot speed, i.e. $v_r = \left(\frac{z}{z+\Delta z}\right) v_r'$

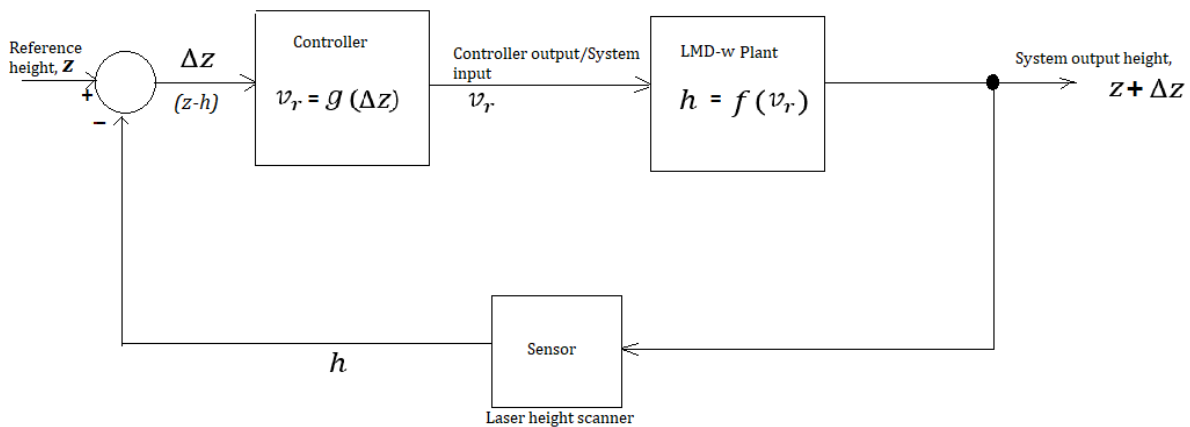


Figure 3-18 - LMD-w process Controller

Let the corrected output height be h . Thus, $h = z + \Delta z$

$$v_r = \left(\frac{z}{h}\right) v_r'$$

$$h = f(v_r) = \left(\frac{z}{v_r}\right) v_r' \quad (3-8)$$

Equation (3-8) is linearized by establishing equilibrium points $\hat{v}_r = v_r'$ and $\hat{h} = z$.

$$h - \hat{h} = K(v_r - \hat{v}_r) \quad (3-9)$$

where

$$K = \left. \frac{df(v_r)}{dv_r} \right|_{v_r = \hat{v}_r = v_r'} = - \left. \frac{z \cdot v_r'}{v_r^2} \right|_{v_r = \hat{v}_r = v_r'} = - \frac{z}{v_r'}$$

$$\therefore h - z = - \frac{z}{v_r'} (v_r - v_r')$$

$$\boxed{h = 2z - \left(\frac{z}{v_r'}\right) v_r} \quad (3-10)$$

Equation (3-10) is the **linearized LMD-w plant**.

3.3.4.2 Derivation of the controller function, $v_r = g(\Delta z)$

In this section, we derive the function $G(s) = \frac{v_r(s)}{\Delta z(s)}$ for the controller shown in Figure 3-18. The time-domain equation is obtained by establishing the value of the robot speed that will yield an output height of $h = z + \Delta z$ as desired.

$$v_r = g(\Delta z) = \left(\frac{z}{z + \Delta z} \right) v_r'$$

At equilibrium points $\widehat{v}_r = v_r'$ and $\widehat{\Delta z} = 0$.

$$v_r - \widehat{v}_r = K(\Delta z - \widehat{\Delta z})$$

where

$$K = \left. \frac{dg(\Delta z)}{d\Delta z} \right|_{\Delta z=0} = - \left. \frac{z \cdot v_r'}{(z + \Delta z)^2} \right|_{\Delta z=0} = - \frac{v_r'}{z}$$

$$\therefore v_r - v_r' = - \frac{v_r'}{z} \Delta z$$

$$\boxed{v_r = v_r' - \left(\frac{v_r'}{z} \right) \Delta z} \quad (3-11)$$

Equation (3-11) is the **linearized controller**.

Figure 3-19 shows the resulting closed-loop system with the controller and plant broken out into constituent process parameters.

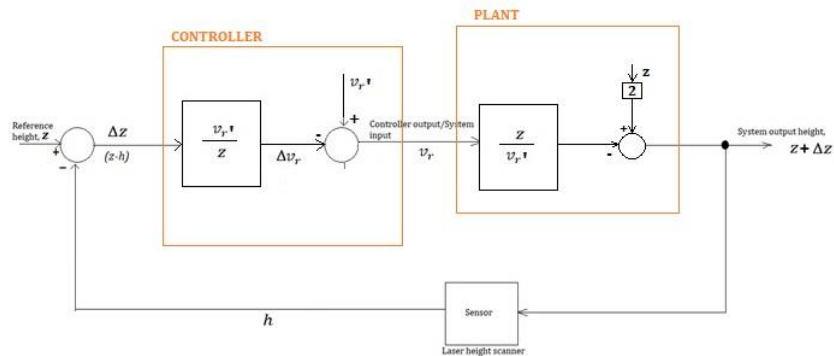


Figure 3-19 - Expanded LMD-w process controller

CHAPTER 4

RESULTS AND DISCUSSION

4.1 Results

4.1.1 Results from open-loop bead width sensing

The tabulated results in Figure 4-1 shows some experimental bead width error measurements for a 150mm bead length, which were logged from the image processing system. In this instance, a tolerance of $\pm 0.5\text{mm}$ was used in flagging an error.

From the results, it can be deduced that the bead profile has 3 erroneous sections: a widening of $\sim 1.3\text{mm}$ a short distance from the start of the bead, a slight narrowing by $\sim 0.6\text{mm}$ beginning from $\sim 65\text{mm}$ into the bead running for about 5mm , and another widening toward the end of the bead from $\sim 123\text{mm}$.

Type	e-Value	DistanceFromOrigin (in mm)
'Bulge'	1.2632	11.6733
'Bulge'	1.2632	12.3407
'Bulge'	1.2105	13.0080
'Bulge'	1.3158	13.6753
'Bulge'	1.3158	14.3427
'Neck'	0.5789	64.3927
'Neck'	0.5789	65.0601
'Neck'	0.5789	65.7274
'Neck'	0.5789	66.3947
'Neck'	0.5789	67.0621
'Neck'	0.5789	67.7294
'Neck'	0.5789	68.3967
'Bulge'	1.1579	123.1181
'Bulge'	1.1579	123.7855
'Bulge'	1.1579	124.4528
'Bulge'	1.1579	125.1201
'Bulge'	1.1579	125.7875
'Bulge'	1.1579	126.4548
'Bulge'	1.1579	127.1221
'Bulge'	0.7368	146.4748
'Bulge'	0.7368	147.1421

Figure 4-1 - Bead width measurements

In-between these sections (indicated by the arrows in Figure 4.1), the bead remains steady within the tolerance range of the target width, for ~50mm and ~ 55mm, respectively. These error amounts, or the e -values, are valuable metrics that can be used in developing a closed-loop control system (also known as a feedback control system), which self-adjusts to compensate for the deviations. It has been found from experimental and analytical approaches that robot travel speed and laser power significantly affect the diameter of a weld bead. Higher powers tend to result in wider and flatter beads, while lower powers yield thin, peaked beads. The width of a bead is also found to be a function of speed, decreasing as deposition speed increases.^[47] Taking the above error data as feedback signals, these relationships can be used to develop the feedback control system, which automatically computes necessary corrective modifications to the process variables and maintains the bead width at its target value.

4.1.2 Results from closed-loop layer height sensing and correction

The figures 4-2 shows the height scan of a layer (of target height 1mm), and to Figure 4-3 shows the error signal $e(t)$ representing height offsets. The adjusted robot speed $v_r(t)$ at which to deposit subsequent layer to compensate for errors is shown in Figure 4-4. Figure 4-5 shows the total output height after correction is implemented. The eventual height after correction will be a sum of the height of the previous layer, $z - \Delta z$, and that of the next layer, $z + \Delta z$, and should result in the target combined height of two layers. Thus, $h_{total} = h_{n-1} + h_n = z - \Delta z + z + \Delta z = 2z$. This is verified in Figure 4-5 where the target layer height is 1mm and the output combined height of the defective and corrected layers is 2mm through the entire length of the bead.

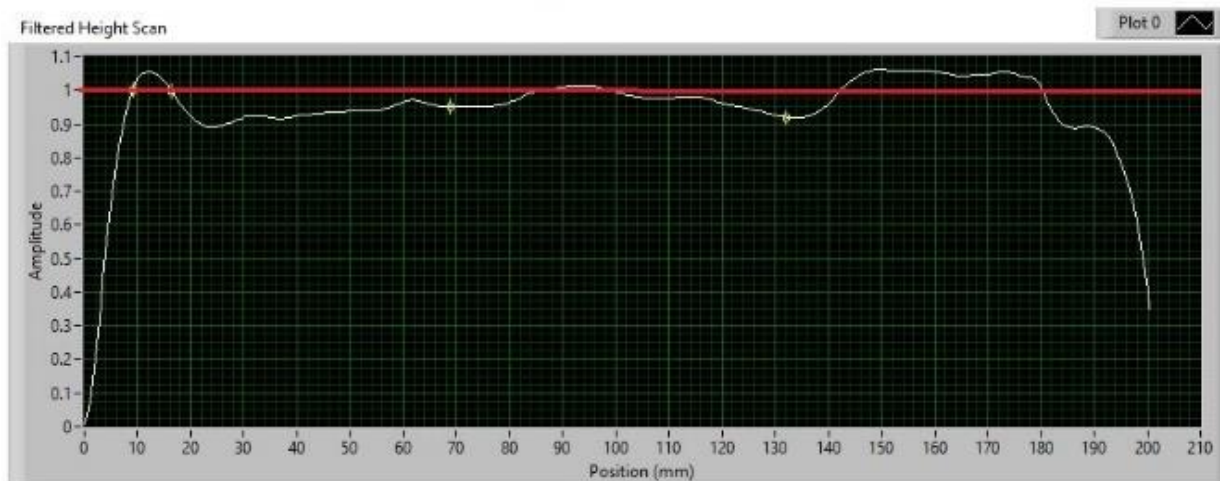


Figure 4-2 - Height scan obtained from laser scanner

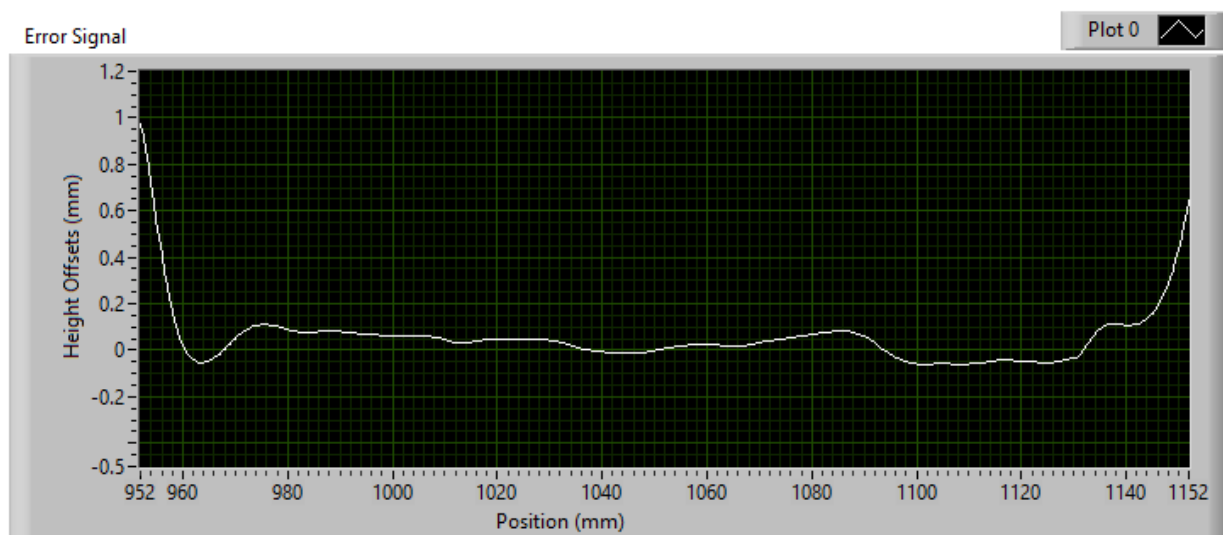


Figure 4-3 - Error signal $e(t)$ representing height offsets

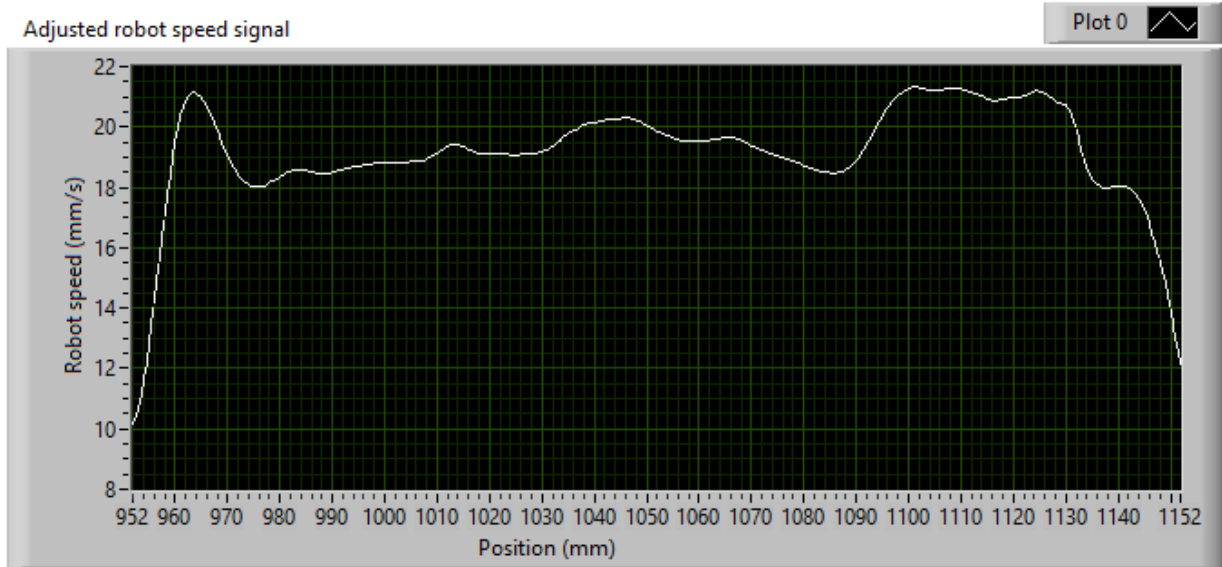


Figure 4-4 - Adjusted robot speed

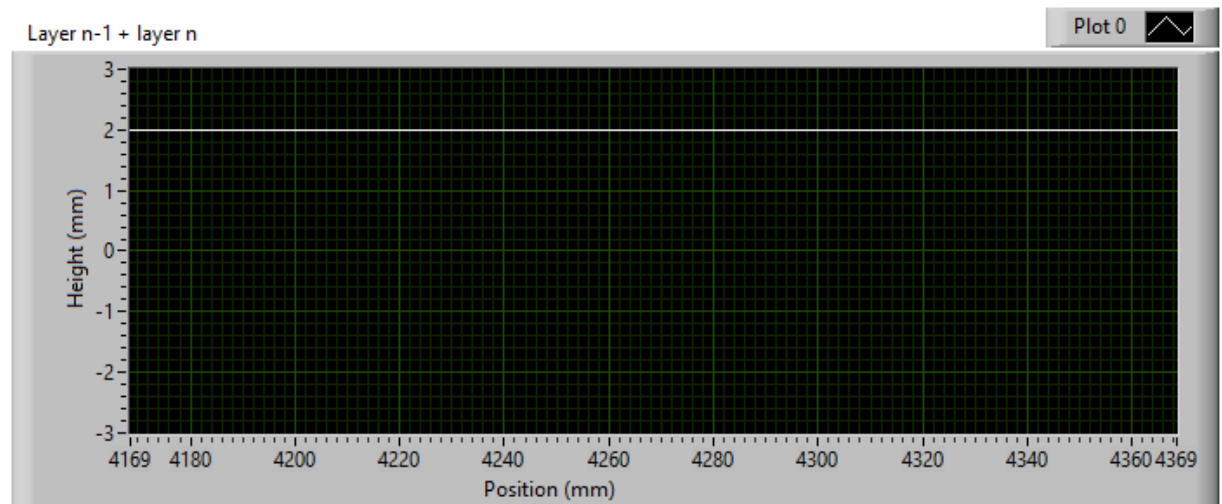


Figure 4-5 - Combined height of the defective and corrected layer, equal to $2 \cdot z$. Target layer height = 1mm. Combined height = 2mm

CHAPTER 5

CONCLUSIONS AND RECOMMENDATIONS

A process monitoring system for wire-fed laser metal deposition has been developed using optical melt pool image processing and laser height scanning. The system includes sensing of bead width errors and feedback correction of layer height offsets from target heights. The closed-loop height control system is evaluated via computer simulation and is verified to adequately compensate for height deviations while depositing a subsequent layer. The open-loop melt pool monitoring system for bead width measurements is evaluated by depositing single beads and analyzing captured images to extract measurement data on the melt pool. The proposed monitoring system features an interactive pre-build calibration of the melt pool region via visual inspection and judgement, enabling the operator to 'teach' the system to correctly identify the melt pool of any build session. The system detects deviations from a target melt pool width and logs error data that can be used in developing a robust automatic error control system through the manipulation of key process variables. It has been found that the bead diameter is significantly dependent on the speed of deposition (i.e. the robot travel speed) and the laser power. In future work, laser power control will be incorporated into the bead width monitoring system and a close-loop control system for bead width using the laser power as the control variable, will be developed. Additional thermal imaging technique using a high-speed infrared camera to capture images from the melt pool will be explored. Information from the analysis of both the optical and thermal images will be fed to the controller and used to adjust the energy source power to ensure uniform temperature distribution. By observing the temperature distribution, process errors originating from insufficient heat dissipation as well as the limits for detecting pores and other irregularities can be studied.

Other key process variables worth noting, and possibly inclusion in a robust control system design, are the wire input speed and the nozzle-to-top-surface distance (NTSD). The development of the automatic error control system following these results and relationships will be studied in future work.

REFERENCES

1. GKNAerospace. *Large Scale Deposition - Laser Wire*. Available from: <http://www.gkngroup.com/additive-manufacturing/processes-applications/GKN-Aerospace/Pages/large-scale-deposition-laser-wire.aspx>.
2. OECD, *The Next Production Revolution Implications for Governments and Business: Implications for Governments and Business*. 2017: OECD Publishing.
3. Alec. *China developing world's largest 3D printer, prints 6m metal parts in one piece*. 2014; Available from: <http://www.3ders.org/articles/20140207-china-developing-world-largest-3d-printer--prints-6m-metal-parts-in-one-piece.html>.
4. Anderson, E., *Additive Manufacturing in China: Aviation and Aerospace Applications (Part 2)*. 2013.
5. Yang, S. *Titanium Alloy 3D Print 2012 China First Invention*. 2013-01-21; Available from: http://www.guancha.cn/shi-yang/2013_01_21_122111.shtml.
6. Kobryn, P.A.O., N.R.; Perkins, L.P.; Tiley, J.S. *Additive Manufacturing of Aerospace Alloys for Aircraft Structures*. in *Cost Effective Manufacture via Net Shape Processing. Meeting Proceedings RTO-MP-AVT-139, Paper 3*. 2006. Neuilly-sur-Seine, France: RTO.
7. Heralic, A., et al. *Visual feed-back for operator interaction in robotized laser metal deposition*. in *Surface Modification Technologies SMT22*. 2008.
8. Tang, L. and R.G. Landers, *Melt Pool Temperature Control for Laser Metal Deposition Processes—Part I: Online Temperature Control*. *Journal of manufacturing science and engineering*, 2010. **132**(1): p. 011010.
9. Tang, L. and R.G. Landers, *Melt Pool Temperature Control for Laser Metal Deposition Processes—Part II: Layer-to-Layer Temperature Control*. *Journal of manufacturing science and engineering*, 2010. **132**(1): p. 011011.
10. Moylan, S., et al., *An additive manufacturing test artifact*. *Journal of research of the National Institute of Standards and Technology*, 2014. **119**: p. 429.
11. ISO841:2001, *Industrial automation systems and integration--Numerical control of machines--Coordinate system and motion nomenclature*. 2001, Geneva, Switzerland.
12. ASTM Standard F2921-11, *Standard Terminology for Additive Manufacturing--Coordinate Systems and Test Methodologies*. 2011: West Conshohocken, PA, ASTM International.
13. Schwerdtfeger, J., R.F. Singer, and C. Körner, *In situ flaw detection by IR-imaging during electron beam melting*. *Rapid Prototyping Journal*, 2012. **18**(4): p. 259-263.
14. Ancona, A., Lugarà, P. M., Ottonelli, F., & Catalano, I. M., *A sensing torch for on-line monitoring of the gas tungsten arc welding process of steel pipes*. *Measurement Science and Technology*, 2004: p. 15(12), 2412.
15. Hofmeister, W.K., Gerald A Maccallum, Danny O, *Video monitoring and control of the LENS process*. 1999, Sandia National Labs., Albuquerque, NM (US); Sandia National Labs., Livermore, CA (US).
16. Hofmeister, W. and M. Griffith, *Solidification in direct metal deposition by LENS processing*. *JOM Journal of the Minerals, Metals and Materials Society*, 2001. **53**(9): p. 30-34.
17. Griffith, M., et al., *Understanding thermal behavior in the LENS process*. *Materials & design*, 1999. **20**(2): p. 107-113.

18. Xiong, J. and G. Zhang, *Adaptive control of deposited height in GMAW-based layer additive manufacturing*. Journal of Materials Processing Technology, 2014. **214**(4): p. 962-968.
19. Lu, W., & Zhang, Y., *Robust sensing and control of the weld pool surface*. 2006: p. 17(9), 2437.
20. Heralić, A., A.-K. Christiansson, and B. Lennartson, *Height control of laser metal-wire deposition based on iterative learning control and 3D scanning*. Optics and lasers in engineering, 2012. **50**(9): p. 1230-1241.
21. Xu, P., Xu, G., Tang, X., & Yao, S., *A visual seam tracking system for robotic arc welding*. The International Journal of Advanced Manufacturing Technology, 2008: p. 37(1-2), 70-75.
22. Bi, G., et al., *Characterization of the process control for the direct laser metallic powder deposition*. Surface and Coatings Technology, 2006. **201**(6): p. 2676-2683.
23. Bi, G., C. Sun, and A. Gasser, *Study on influential factors for process monitoring and control in laser aided additive manufacturing*. Journal of Materials Processing Technology, 2013. **213**(3): p. 463-468.
24. Boddu, M.R., et al. *Empirical modeling and vision based control for laser aided metal deposition process*. in *Proceedings of the Solid Freeform Fabrication Symposium*. 2001.
25. Tapia, G. and A. Elwany, *A review on process monitoring and control in metal-based additive manufacturing*. Journal of Manufacturing Science and Engineering, 2014. **136**(6): p. 060801.
26. Krauss, H., C. Eschey, and M. Zaeh. *Thermography for monitoring the selective laser melting process*. in *Proceedings of the Solid Freeform Fabrication Symposium*. 2012.
27. Hu, D. and R. Kovacevic, *Sensing, modeling and control for laser-based additive manufacturing*. International Journal of Machine Tools and Manufacture, 2003. **43**(1): p. 51-60.
28. Hu, D. and R. Kovacevic, *Modelling and measuring the thermal behaviour of the molten pool in closed-loop controlled laser-based additive manufacturing*. Proceedings of The Institution of Mechanical Engineers, Part B: Journal of Engineering Manufacture, 2003. **217**(4): p. 441-452.
29. Heralić, A., et al., *Increased stability in laser metal wire deposition through feedback from optical measurements*. Optics and Lasers in Engineering, 2010. **48**(4): p. 478-485.
30. Medrano, A., et al. *Fibre laser metal deposition with wire: parameters study and temperature monitoring system*. in *XVII International Symposium on Gas Flow and Chemical Lasers and High Power Lasers*. 2008. International Society for Optics and Photonics.
31. Iravani-Tabrizipour, M. and E. Toyserkani, *An image-based feature tracking algorithm for real-time measurement of clad height*. Machine Vision and Applications, 2007. **18**(6): p. 343-354.
32. Toyserkani, E. and A. Khajepour, *A mechatronics approach to laser powder deposition process*. Mechatronics, 2006. **16**(10): p. 631-641.
33. Bi, G., et al., *Identification and qualification of temperature signal for monitoring and control in laser cladding*. Optics and lasers in engineering, 2006. **44**(12): p. 1348-1359.
34. Bi, G., et al., *Development and qualification of a novel laser-cladding head with integrated sensors*. International Journal of Machine Tools and Manufacture, 2007. **47**(3): p. 555-561.

35. Mazumder, J., et al., *Closed loop direct metal deposition: art to part*. Optics and Lasers in Engineering, 2000. **34**(4): p. 397-414.
36. Tang, L., et al., *Variable powder flow rate control in laser metal deposition processes*. Journal of Manufacturing Science and Engineering, 2008. **130**(4): p. 041016.
37. Doubenskaia, M., P. Bertrand, and I. Smurov, *Optical monitoring of Nd: YAG laser cladding*. Thin Solid Films, 2004. **453**: p. 477-485.
38. Hua, T., et al., *Research on molten pool temperature in the process of laser rapid forming*. journal of materials processing technology, 2008. **198**(1): p. 454-462.
39. Tan, H., et al., *Estimation of laser solid forming process based on temperature measurement*. Optics & Laser Technology, 2010. **42**(1): p. 47-54.
40. Sciaky. *Advantages of Wire AM vs. Powder AM*. Available from: <http://www.sciaky.com/additive-manufacturing/wire-am-vs-powder-am>.
41. Abdullah, B., et al. *Monitoring of TIG welding using laser and diode illumination sources: A comparison study*. in *Electronic Design, 2008. ICED 2008. International Conference on*. 2008. IEEE.
42. Eriksson, I., et al., *New high-speed photography technique for observation of fluid flow in laser welding*. Optical Engineering, 2010. **49**(10): p. 100503-100503-3.
43. INOuE, K., *Image Processing for On-Line Detection of Welding Process (Report III): Improvement of Image Quality by Incorporation of Spectrum of Arc*. Transactions of JWRI, 1981. **10**(1): p. 13-18.
44. KIM, E., C. Allemand, and T. EAGAR, *Visible light emissions during gas tungsten arc welding and its application to weld image improvement*. micron, 1987. **500**(250): p. 100.
45. Ogawa, Y., *Visual Analysis of Welding Processes*. 2012: INTECH Open Access Publisher.
46. Photron, *Slow motion analysis of different welding techniques*, in *Arc welding Videos*. 2014, Photron Marketing.
47. Tadamalle, A., Y. Reddy, and E. Ramjee, *Influence of laser welding process parameters on weld pool geometry and duty cycle*. Advances in Production Engineering & Management, 2013. **8**(1): p. 52.

VITA

Adeola Adediran earned her Bachelor of Science in Computer Engineering from University of Lagos, Nigeria in 2012. For her undergraduate thesis, she worked on an independent project to design a remote-control system for large industrial machinery. In 2011, she joined Chevron Nigeria briefly as an Instrumentation intern working on production platform control instruments, particularly piezoelectric sensors and transmitters on off-shore platforms.

Her primary research interest is incorporating innovations in robotics and automation technologies into manufacturing to tackle the problem of energy inefficiency in the manufacturing industry. She is currently working with Lonnie Love at the National Transportation Research Center (NTRC) of the Oak Ridge National Laboratory on exploring the possibility of large scale metal additive manufacturing through laser metal deposition with wire (LMD-w), a technique that builds metal structures by using a laser to melt metal wire into beads onto a substrate layer by layer, and an industrial 6-Degree-of-Freedom robotic manipulator to provide positioning of the print head. Her current project is developing a robust process control for automatic defect detection and correction in the LMD-w process. The research goal is to reduce stock material waste to yield substantial cost and energy savings in manufacturing, with focus on the aerospace industry.